

Angiotensin II regulates phosphorylation of actin-associated proteins in human podocytes

Laura K. Schenk,^{*,1} Annika Möller-Kerutt,^{*,1} Rafael Klosowski,^{†,1} Dirk Wolters,[†] Elisabeth Schaffner-Reckinger,[‡] Thomas Weide,^{*} Hermann Pavenstädt,^{*,1} and Beate Vollenbröker^{*,1,2}

^{*}Medizinischen Klinik und Poliklinik D, Universitätsklinikum Münster, Münster, Germany; [†]Analytische Chemie, Biomolekulare Massenspektrometrie, Ruhr-Universität Bochum, Bochum, Germany; and [‡]Laboratory of Cytoskeleton and Cell Plasticity, Life Sciences Research Unit, University of Luxembourg, Esch-sur-Alzette, Luxembourg

ABSTRACT: Within the kidney, angiotensin II (AngII) targets different cell types in the vasculature, tubuli, and glomeruli. An important part of the renal filtration barrier is composed of podocytes with their actin-rich foot processes. In this study, we used stable isotope labeling with amino acids in cell culture coupled to mass spectrometry to characterize relative changes in the phosphoproteome of human podocytes in response to short-term treatment with AngII. In 4 replicates, we identified a total of 17,956 peptides that were traceable to 2081 distinct proteins. Bioinformatic analyses revealed that among the increasingly phosphorylated peptides are predominantly peptides that are related to actin filaments, cytoskeleton, lamellipodia, mammalian target of rapamycin, and MAPK signaling. Among others, this screening approach highlighted the increased phosphorylation of actin-bundling protein, L-plastin (LCP1). AngII-dependent phosphorylation of LCP1 in cultured podocytes was mediated by the kinases ERK, p90 ribosomal S6 kinase, PKA, or PKC. LCP1 phosphorylation increased filopodia formation. In addition, treatment with AngII led to LCP1 redistribution to the cell margins, membrane ruffling, and formation of lamellipodia. Our data highlight the importance of AngII-triggered actin cytoskeleton-associated signal transduction in podocytes.—Schenk, L. K., Möller-Kerutt, A., Klosowski, R., Wolters, D., Schaffner-Reckinger, E., Weide, T., Pavenstädt, H., Vollenbröker, B. Angiotensin II regulates phosphorylation of actin-associated proteins in human podocytes. *FASEB J.* 31, 000–000 (2017). www.fasebj.org

KEY WORDS: kidney · L-plastin · actin turnover · calcium

The glomerular filtration barrier in the kidney is among those composed of podocytes with interdigitating actin-based processes. These podocyte foot processes with the interposed slit diaphragm play an important role in maintaining the selective permeability of the glomerular filtration barrier that retains large proteins but freely filters water, electrolytes, and small molecules (1). During the last decade, it has become clear that podocyte injury is associated with proteinuria (1–3).

The peptide hormone, angiotensin II (AngII), is a major component of the renin-angiotensin-aldosterone system (RAAS) and, thus, a crucial regulator of blood pressure, salt-water balance, sympathetic nervous system, and

tissue homeostasis (4). AngII mediates the vasoconstriction of the efferent glomerular arteriole, thereby physiologically regulating the glomerular filtration rate (5). High levels of AngII and sustained RAAS activation are crucial factors in the pathogenesis of glomerular injury (6), and AngII is a major profibrotic cytokine that leads to glomerulosclerosis (7). Clinical studies have proven that AngII receptor 1 (AT1R) blocker and angiotensin-converting enzyme inhibitors have a beneficial effect on proteinuria and inhibit the progression of kidney disease (8). Indeed, administration of these drugs is associated with lower mortality in patients with chronic kidney disease (9).

The AngII receptor, AT1R, is a GPCR. Upon receptor activation *via* AngII stimulation, the intracellular C terminus of AT1R couples to G proteins, such as G_{q/11}, G_i, G₁₂, and G₁₃, thereby inducing various second messenger pathways, such as PLC/inositol trisphosphate, reactive oxygen species, calcium, and protein kinase signaling (10, 11). It has also been shown that AngII has direct effects on the actin cytoskeleton rearrangement of podocytes. The integrity of the actin cytoskeleton is important for the physiologic function of podocytes, and actin cytoskeleton deregulation may result in podocyte disease (12);

ABBREVIATIONS: AngII, angiotensin II; AT1R, angiotensin II receptor type 1; LCP1, L-plastin; RAAS, renin-angiotensin-aldosterone system; RFP, red fluorescent protein; RSK, p90 ribosomal S6 kinase; SILAC, stable isotope labeling with amino acids in cell culture; WT, wild type

¹ These authors contributed equally to this work.

² Correspondence: Medizinischen Klinik und Poliklinik D, Albert Schweitzer Campus 1, A14, D-48149 Münster, Germany. E-mail: beate.vollenbroeker@ukmuenster.de

doi: 10.1096/fj.201700142R

This article includes supplemental data. Please visit <http://www.fasebj.org> to obtain this information.

however, the molecular details of AngII-dependent signaling cascades in podocytes are not yet fully understood. In this study, we focused on AT1R-mediated protein kinase signaling and investigated which phosphorylation sites were regulated during short-term treatment with AngII in AT1R-expressing human podocytes.

Our data analyses revealed an over-representation of actin-associated proteins among regulated phosphorylation sites. Among other proteins, AngII stimulation induced the phosphorylation of L-plastin (LCP1). The actin bundling protein, LCP1, is known for its important role in the regulation of the actin cytoskeleton of leukocytes and solid tumor cells (13), and we now can add several novel aspects of LCP1 regulation in podocytes.

MATERIALS AND METHODS

Cell culture and stable isotope labeling with amino acids in cell culture

Human immortalized podocytes (AB8/13; kindly provided by M. Saleem, School of Clinical Sciences, University of Bristol, Bristol, United Kingdom), the Retro-X packing cell line GP2-293, and HEK293 cells (Thermo Fisher Scientific, Waltham, MA, USA) were cultivated at standard conditions as previously described (14, 15). Generation and characterization of stably transfected AB8 3F-AT1R cell lines has been previously described (14). For relative quantification of the phosphoproteome, AB8 3F-AT1R podocytes were grown in stable isotope labeling with amino acids in cell culture (SILAC) (16) culture medium that contained amino acids arginine and lysine labeled with stable isotopes (heavy: [¹³C]₆ [¹⁵N]₄ arginine, [¹³C]₆ lysine; light: [¹²C]₆ [¹⁴N]₄ arginine, [¹²C]₆ lysine) for 3 passages. This labeling period is sufficient to achieve >98% saturation of labeling (17). On the day of the experiment, 1 set of cells was treated with AngII (100 nM for 15 min; Sigma-Aldrich, St. Louis, MO, USA), another with vehicle, and then samples were pooled 1:1 (AngII/vehicle). In 2 biological replicates, cells that were grown in medium with heavy isotopes of amino acids were treated with AngII, and in 2 replicates cells that were grown in light isotopes were treated.

Sample purification and liquid chromatography–tandem mass spectrometry

After filter-aided sample preparation (18), TiO₂ microcolumn phosphopeptide enrichment was performed (19). Samples were loaded on MudPIT columns as previously described (20). Kinetex C₁₈ (Phenomenex, Torrance, CA, USA) was used as material for reversed phase chromatography. The HPLC program consisted of 17 varying steps with 200 min each, culminating in a total duration of 30 h. The first 3 steps used a linear gradient of acetonitrile only (buffer B: 0.1% formic acid; buffer A: H₂O) followed by 11 salt steps with the concentration increased 10% each for buffer C (250 mM ammonium acetate), with linear acetonitrile gradients in between. Three steps of high buffer D (1.5 M ammonium acetate) concentration followed at the end. The following parameters were used for the mass spectrometric analysis *via* LTQ Orbitrap velos (Thermo Fisher Scientific): ionization voltage of 1.8 kV; capillary temperature of 200°C; tandem mass spectrometry fragmentations of the 20 most intense signals; dynamic mass exclusion of 60 s; maximum orbitrap fill time of 500 ms in positive ion mode; maximum ion trap fill time of 100 ms; and collision-induced dissociation at 35 V. Collected data were filtered and examined by using MaxQuant software (21). The following parameters differ from the standard settings of

MaxQuant 1.5.2.8: decoy mode reward; minutes score for modified peptides 0; minutes δ score for modified peptides 0; and discard unmodified counterpart peptides false. In total, we analyzed 4 biological replicates with 3 technical replicates each. After peptide assignment using MaxQuant software as specified above, results from all 12 samples were compiled in 1 spreadsheet.

Peptides were crosschecked to exclude ambiguous protein assignments. In total, 17,956 peptide assignments were included in the analyses. The median of all peptide quantifications was 1.01. For additional analyses, we focused on subsets of peptides, specifically those with altered abundance upon treatment with AngII. To get a general impression, a liberal cutoff of phosphopeptide ratios of >1.5 or <0.67 for increase or decrease, respectively, was chosen [in parallel with Lefkowitz and colleagues (22)]. Of peptides, 15,242 had an AngII-to-vehicle ratio of >0.67 and <1.5. Four hundred sixty-five peptide ratios were <0.67, and 2249 were >1.5. Supplemental Table 1 gives a transparent overview of peptide abundance and quantification result.

Functional analyses

Functional annotation was performed with David Gene Ontology (<https://david.ncifcrf.gov/summary.jsp> and <http://reactome.org>) (23). These databases provide information about gene and protein attributes that are chiefly obtained by data mining and that enable the user to perform enrichment analyses. Phosphosite analyses were performed with PhosphoLogo (<https://hpcwebapps.cit.nih.gov/PhosphoLogo/>) (24). Kinase substrates were analyzed in comparison with phosphosite analyses (<http://www.phosphosite.org/>) (25).

Western blot

Immunoblotting was carried out as described previously (14, 26). Antibodies for ERK, phospho-ERK1/2, GAPDH, phospho-p90 ribosomal S6 kinase (RSK) T359, and RSK1/2/3 were from Cell Signaling Technology (Danvers, MA, USA). Abs for actin, β -tubulin, FLAG, and FLAG (M2) were obtained from Sigma-Aldrich. Ab against LCP1 was obtained from Thermo Fisher Scientific. The generation of the Ab against phospho-LCP1 (Ser5) was described previously (27). All primary Abs with the exception of LCP1 (1:200) were used in a 1:1000 dilution.

Where indicated, cells were treated with AngII, ATP, losartan, and LPS (all from Sigma-Aldrich); Rp-8-Br-cAMP (Biolog, Bremen, Germany); U0126 (Cell Signaling Technology); BID1870 (Enzo Life Sciences, Lörrach, Germany); or GF109203 (Cayman Chemical, Ann Arbor, MI, USA).

Quantification of Western blot signals

Signals that were derived from the same immunoblot were densitometrically quantified by using ImageJ (National Institutes of Health, Bethesda, MD, USA). Quotients from signals of phospho-specific Abs and from the complete amount of protein are shown. Evaluation was performed by using GraphPad Prism (GraphPad Software, La Jolla, CA, USA). All data show the SD of at least 3 independent experiments and were analyzed by using unpaired Student's *t* test.

Immunofluorescence

Staining was performed as previously described (14). Abs against LCP1 (1:100) and Alexa Fluor 488 Phalloidin (1:200) were purchased from Thermo Fisher Scientific. Ab against T-plastin (1:50)

was from GeneTex (Irvine, CA, USA). Samples were examined with an Axio Observer Z1 microscope and ApoTome technology (Carl Zeiss AG, Oberkochen, Germany; objective: EC Plan Neofluar $\times 40/1.30$ Oil DIC M27) using Axio Vision 4.7.

Aggregation assay

AB8 3F-AT1R cells were detached by using Accutase (Sigma-Aldrich) and diluted in aggregation buffer (1.25 mM CaCl_2 , 10 mM HEPES, 0.1% bovine serum albumin at physiologic osmolarity and pH) to a density of 6×10^5 cells/ml. Cells were allowed to aggregate during shaking (80 rpm, 33°C) with or without the addition of 100 nM AngII. Cell diameter, single cells, and cell aggregates of treated and control cells were calculated with the Luna Cell Counter (Logos Biosystems, Villeneuve d'Ascq, France) after 0 and 30 min of incubation.

Cloning of LCP and T-plastin mutants and transfection

Human LCP1 cDNA was amplified from a human immortalized podocyte library (LCP1_fwd: 5'-CACCGGGCGCGCCATGGC-CAGAGGATCA GTGTCCGATGAG-3', LCP1_rev: 5'-TTAAT-TAATCACACCCTCTTCATTCCTTCC-3'), inserted into pENTR-D/TOPO vector and then cloned into the pmRFP-C2 vector [backbone manufacturer: R. Y. Tsien (28)], which allows the visualization of red fluorescent protein (RFP)-tagged LCP1 in fixed cells and in live cell experiments. Phosphorylation variants LCP1 S5A and LCP1 S5E were generated by using different forward primers during amplification, changing Ser5 into alanine (S5A: 5'-CACCGGGCGCGCCATGGCCAGAGGAGCAGTG-TCCGATGAG-3') or changing Ser5 into glutamic acid (S5E: 5'-CACCGGGCGCGCCATGGCCAGAGGAGAAGTCCGATGAG-3'). Deletion mutants were cloned with primers binding behind the LCP1 EF hand motifs, LCP1_minusEF (5'-CACCGG-GCGCGCCGATGTTGCCAAGACCTTTAGAAAAGC-3'), amplifying AA 85–628, or LCP1_phospho_minusEF (5'-CACCGGGCGCGCCATGGCCAGAGGATCAGTGTCCGATGAGAAAATGATGAGCTCAGAGATGTTGCCAAGACCTTTAGAAAAGC-3'), amplifying AA 1–15 + 85–628. Human T-plastin cDNA was also amplified from the human immortalized podocyte library by using the primers WT_fwd (5'-CACCGGGCGCGCCATGGATGAGATGGCTACCACTCA-GATT-3') and WT_rev (5'-TTAATTAATTACTCTCTTCATTC-CCCTGCC-3'). For amplification of the deletion mutant, T-plastin_minusEF, the forward primer was replaced with the primer minusEF_fwd (5'-CACCGGGCGCGCCATTGCCAA-GACCTTCCGCAAAGCAATCAACAGG-3'). Amplified DNA was also cloned into the pmRFP-C2 vector. Transient transfection of podocytes was performed by using Lipofectamine 2000 (Thermo Fisher Scientific) according to the manufacturer's instructions.

Quantification of filopodia length and amount

RFP signals in immunofluorescence images of cells transfected with pRFP-LCP1-WT (wild-type), pRFP-LCP1-S5A, pRFP-LCP1-S5E, and pEGFP-C2 empty vector (mock) were analyzed by using the filopodia code in MatLab (MathWorks, Natick, MA, USA) as described in detail by Nilufar *et al.* (29). The number of filopodia per cell and the average length of filopodia in transfected cells were calculated.

Live cell imaging

For live cell imaging, AB8 3F-AT1R podocytes were seeded on an Ibidi μ -Dish 35-mm high with glass bottom (Ibidi, Martinsried,

Germany) and transiently transfected with the different pmRFP-LCP1 or pmRFP-T-plastin constructs. Using the microscope mentioned above, approximately 40 time-lapse images of transfected cells 48 h after transfection were taken every 20 s, starting with stimulation with 100 nM AngII directly under the microscope after the fifth image (video time, 13 min). An additional end point photo was obtained 15 min after stimulation. For blockade of AT1R, transfected cells were preincubated for 2 h with losartan (10 μM) or for inhibition of RSK with BID-1870 (10 μM) for 3 h before the start of experiments. For Ca^{2+} -reduced conditions, cells were incubated with BAPTA-AM (10 μM , 1 h; AAT Bioquest, Sunnyvale, CA, USA) to complex intracellular Ca^{2+} ions. Furthermore, extracellular calcium concentration was reduced to 0.8 mM by adding an adequate amount of Ca^{2+} -free Krebs-Ringer solution (145 mM NaCl, 1.6 mM K_2HPO_4 , 0.4 mM KH_2PO_4 , 5 mM glucose, 1 mM MgCl_2 , 5 mM EGTA).

RESULTS

AngII leads to quantitative changes in the phosphoproteome of human podocytes

We chose an immortalized human podocyte cell line (AB8/13) with robust expression of FLAG-tagged AT1R (AB8 3F-AT1R) as a model system (14). These cells resemble podocytes *in vivo* with regard to their expression of podocyte-specific cytoskeletal proteins, nephrin and synaptopodin (30). Moreover, they can form filopodia and lamellipodia and, as a result of their large size, they are excellent targets for the visualization of intracellular processes.

Temporal dynamics of phosphorylation events upon GPCR activation are highly complex (31–33); therefore, we performed time course experiments and demonstrated the phosphorylation of ERK within the first 15 min after AngII stimulation (14). Thus, we chose this time point for our proteomic study.

Relative quantification of AngII-dependent changes of the cellular phosphoproteome was performed by using SILAC coupled with phosphopeptide enrichment and liquid chromatography–tandem mass spectrometry (Supplemental Fig. 1A). Accordingly, AB8 3F-AT1R cells that were grown in SILAC culture media were treated with AngII (100 nM) or vehicle for 15 min. An effective AngII stimulation was demonstrated by increased ERK phosphorylation in a Western Blot (Supplemental Fig. 1B). Subsequently, cell extracts were used for sample preparation, including phosphopeptide enrichment, mass spectrometry, bioinformatic peptide assignment, and semiquantitative quantification. With this approach, we identified 17,956 peptides in 4 biological replicates, each performed in 3 technical replicates. A total of 4951, 4729, 5173, and 3103 phosphopeptides was found, corresponding to 1494, 1209, 1224, and 891 phosphoproteins—in replicates 1, 2, 3, and 4, respectively (Fig. 1 and Supplemental Fig. 1C). After removal of redundant peptides, 6323 unique phosphopeptides could be traced back to 2081 distinct proteins. A large proportion of 1326 proteins were found in at least 2 of the experiments (Fig. 1A). We observed increased and decreased amounts of phosphopeptides upon 15 min of treatment with AngII (Fig. 1B). Among the identified phosphorylation sites, $\sim 90\%$ were

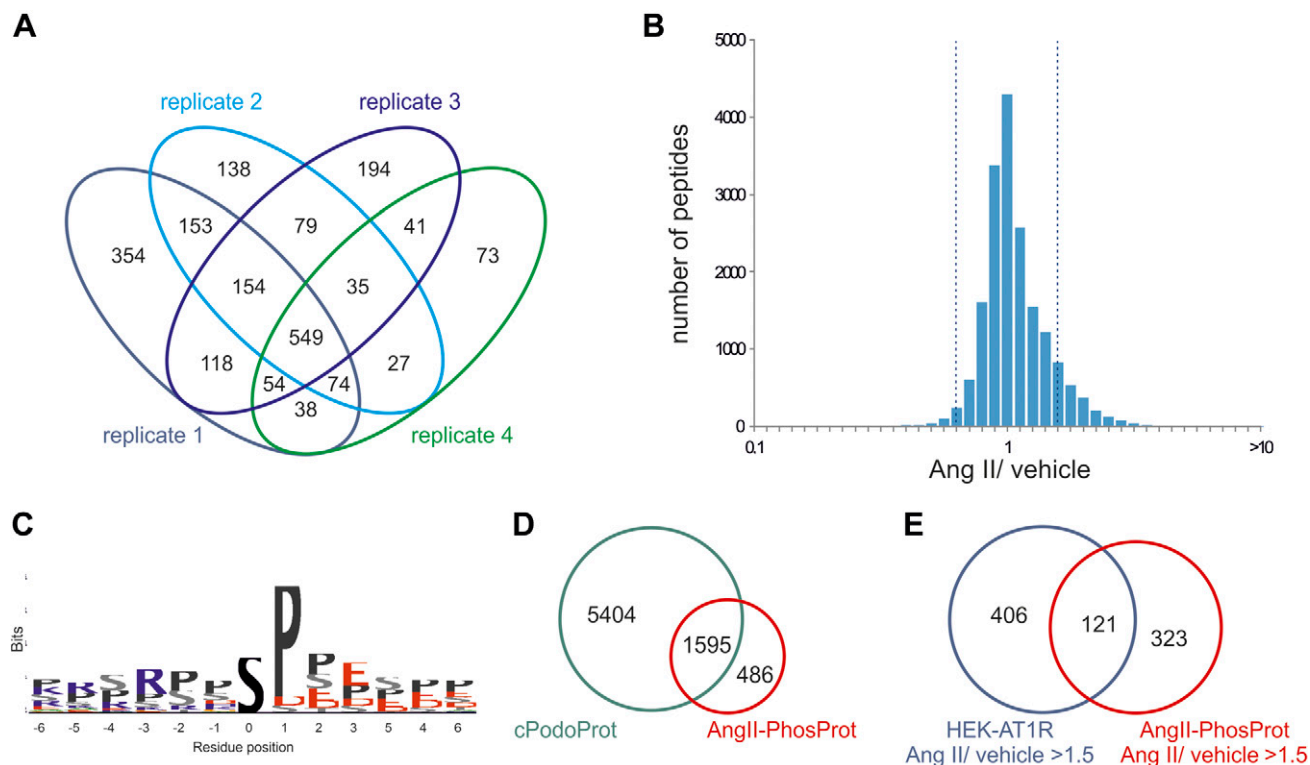


Figure 1. Characterization and quantitation of AngII-induced regulation of the phosphoproteome in human immortalized podocytes. *A*) Venn diagram of the 2081 unique protein assignments in 4 biological replicates of AB8 3F-AT1R cells. A total of 1494, 1209, 1224, and 891 phosphoproteins were found in replicates 1, 2, 3, and 4, respectively. *B*) Histogram of the distribution of peptide ratios comparing podocytes that were treated with AngII (100 nM; 15 min) *vs.* vehicle. For additional analyses, a liberal cutoff of phosphopeptide ratios of >1.5 or <0.67 for increase or decrease, respectively, was chosen. *C*) Analysis of the phosphorylation site sequence motif, depicted for all peptides with a >1.5 AngII-to-vehicle ratio was performed with PhosphoLogo. *D*) Venn diagram of all proteins identified in this study (AngII-PhosProt) compared with a non-phospho-enriched proteome characterization of primary murine podocytes (cPodoProt) from Rinschen *et al.* (33). *E*) Venn diagram comparing the phosphoproteins that were increased in this study (AngII-PhosProt) compared with phosphoproteins that were increased in a study of AT1R signaling in HEK293 cells (HEK-AT1R) from Christensen *et al.* (34).

phosphoserine, ~9% phosphothreonine, and ~1% phosphotyrosine. Phosphosite analysis demonstrated that treatment of podocytes with AngII for 15 min led to an increased serine/threonine phosphorylation at proline-directed sites (proline at position +1), which fits to a motif that is predominantly used in MAPK signaling (Fig. 1C). This sequence motif preference was reproducible for both $>1.5\times$ and $>3\times$ increased AngII/vehicle phosphopeptide ratios. We next compared our data with other studies in this field. A large proportion of the proteins that we identified in our samples have been repeatedly found in other renal phosphoproteomic databases, but, in addition, we could identify several novel phospho-targets of AT1R signaling in podocytes. In comparison to other studies, it is interesting to overlap the phosphoproteins identified in the podocyte cell line in our study with native glomerular podocytes, and to evaluate parallels with studies that characterized AngII-induced phosphoproteomic changes in different cell types. Of proteins, 1595 from our screen have previously been proven to be expressed in podocytes by a non-phospho-enriched proteome characterization of primary cultured murine podocytes (34) (Fig. 1D). In another study, the relative quantification of the AngII-dependent phosphoproteome of AT1R-expressing

HEK293 cells was performed (35). One hundred twenty-one of the phosphoproteins that were increased in our study were also regulated in HEK293 cells (35), whereas 323 proteins were apparently podocyte-specific targets of AngII phospho-signaling (Fig. 1E).

AngII increased phosphorylation of actin filament-associated peptides

To get a general impression, a liberal cutoff of phosphopeptide ratios of >1.5 or <0.67 for increase or decrease, respectively, was chosen [in parallel to Lefkowitz and colleagues (22) and Christensen *et al.* (35)].

With these criteria, 85% of the total 17,956 peptides had an AngII-to-vehicle ratio of >0.67 and <1.5 , which was resumed as unregulated, in 2.5% the peptide ratio was decreased (<0.67) and in 12.5% the ratio was increased (>1.5). Four hundred twenty-six unique phosphorylation sites were increased, 1560 were unchanged, and 41 were decreased. Supplemental Table 1 provides an overview of all peptide abundances and a quantification of results. Phosphopeptides with the largest relative increase in abundance belonged to the proteins tenascin, integrin- $\beta 6$,

neuroblast differentiation-associated protein, LCP1, optineurin, plasminogen activator inhibitor 1, serine/threonine protein kinase D2, protein bicaudal C homolog 1, phalloidin, and ephrin type-A receptor 2. **Table 1** summarizes the 10 phosphopeptides with the largest increase in abundance.

Quantitative changes in protein phosphorylation often reflect the activation of distinct cellular signaling processes. Indeed, most of the increased phosphopeptides from our screen were part of signal transduction pathways (**Fig. 2A**). Next, gene ontology analyses and functional classifications were used to screen our phosphoproteomic results and to classify the regulated phosphopeptides—we used the Database for Annotation, Visualization, and Integrated Discovery (DAVID) Gene Ontology database (<http://david.abcc.ncifcrf.gov>). This approach revealed that phosphopeptides that were related to actin filaments, lamellipodia, and cell leading edge were over-represented among the increasingly phosphorylated peptides (**Fig. 2B**). Furthermore, phosphorylation of proteins that influence molecular functions, such as intramolecular transferase activity and Rho GTPase activator activity, was increased after AngII stimulation (**Fig. 2C**). With regard to signaling pathways and biological processes, mammalian target of rapamycin signaling, glucose metabolism, and focal adhesion were over-represented (**Supplemental Fig. 2A, B**).

On the basis of the over-representation of actin-associated pathways in our analyses and the great importance of actin cytoskeletal dynamics for podocytes, we took a closer look at this group of proteins and identified many phosphopeptides from proteins that were linked with the actin cytoskeleton (**Table 2**). A schematic overview of phosphoproteins related to the gene ontology terms, actin filaments, lamellipodia, and cell leading edge is given in **Fig. 2D**.

AngII-induced LCP1 phosphorylation is mediated by the kinases RSK, PKA, and PKC

Phospho-Ser5 LCP1 was one of the most enriched peptides in our phosphoproteomic screen after 15 min of AngII treatment in human podocytes (**Table 1**). The protein LCP1 is one of 3 plastin isoforms that are found in mammalian cells that belong to the α -actinin family

of actin cross-linking proteins, which play a crucial role in podocyte biology. Indeed, mutations in the protein α -actinin-4, for example, have previously been linked to podocyte injury (36). In contrast to other α -actinin family members, plastins have 2 actin-binding domains in a single polypeptide chain. Cross-linking parallel actin filaments into tight bundles, plastins can stabilize larger-order F-actin structures. On the one hand, the bundling activity of LCP1 is regulated by calcium binding at EF-hand loops and, on the other, by serine phosphorylation sites, both of which are included in the N-terminal region of LCP1 (13).

First, AngII-induced phosphorylation of LCP1 at Ser5 (p-LCP1) was replicated in Western blot experiments with a highly specific Ab against this phosphorylation site (27). Total LCP1 abundance remained unchanged (**Supplemental Fig. 3**). AngII-dependent phosphorylation of ERK at the activating Thr202/Tyr204 site (p-ERK) served as control for stimulation, and the stable expression of 3F-AT1R served as control of the cell line. Evaluation of 4 independent experiments allowed quantification of the AngII-dependent increase of LCP1 and ERK phosphorylation, shown as a ratio of phosphorylated proteins and the total amount of proteins (**Supplemental Fig. 3**).

It is known that the extracellular stimulation of AT1R with AngII increases the level of intracellular calcium and, in part as a consequence, leads to the activation of several kinases, which transfers additional signal transduction (10, 11). In additional experiments, we examined the signaling pathway of AngII-induced LCP1 phosphorylation. To investigate whether an AngII-induced Ca^{2+} influx is primarily responsible for LCP1 phosphorylation, we treated cells with ionomycin, which elicits a large Ca^{2+} increase in the cytoplasm of cells (37); however, an increase in intracellular Ca^{2+} alone did not lead to an increase in p-LCP1 (**Fig. 3A**). Treatment with a high concentration of ATP, which, similar to AngII, leads to a G protein-induced increase of intracellular Ca^{2+} , could, in contrast, induce the phosphorylation of LCP1 and that of kinases ERK and RSK (p-RSK). LPS is known as a podocyte-affecting substance, which leads *in vivo* to foot process effacement and damage to the slit diaphragm (38). To examine whether podocyte damage in general leads to LCP1

TABLE 1. Compilation of the 10 peptides with the largest increase in peptide ratio upon AngII stimulation (100 nM; 15 min) vs. control

Protein name	Gene symbol	Mean Ang/Ktr	Sequence	Modification site
Tenascin-N	TNN	29.45	Y*VVRY*T*SAGGETR	Y650, Y654; T655
Integrin- β 6	ITGB6	13.22	VGDT*AS*FSVT*VNIPHCER	T414; S416; T420
Neuroblast differentiation-associated protein AHNAK	AHNAK	8.09	LKS*EDGVEGDLGETQSR	S135
L-Plastin	LCP1	7.09	GS*VSDEEMMELR	S5
Optineurin	OPTN	5.40	HGARTS*DSDQQAYLVQR	S520
Plasminogen activator inhibitor 1 RNA-binding protein	SERBP1	5.38	S*KSEEAHAEDSVMDHHFR	S313
		5.26	S*KS*EEAHAEDSVMDHHFR	S313; S315
Serine/threonine-protein kinase D2	PRKD2	4.25	RLS*STSLAS*GHSVR	S197; S203
Protein bicaudal C homolog 1	BICC1	4.21	S*PSHSGNAGDLK	S633
Palladin	PALLD	4.17	IAS*DEEIQGTK	S669
Ephrin type-A receptor 2	EPHA2	4.08	LPS*TSGSEGVVPR	S897

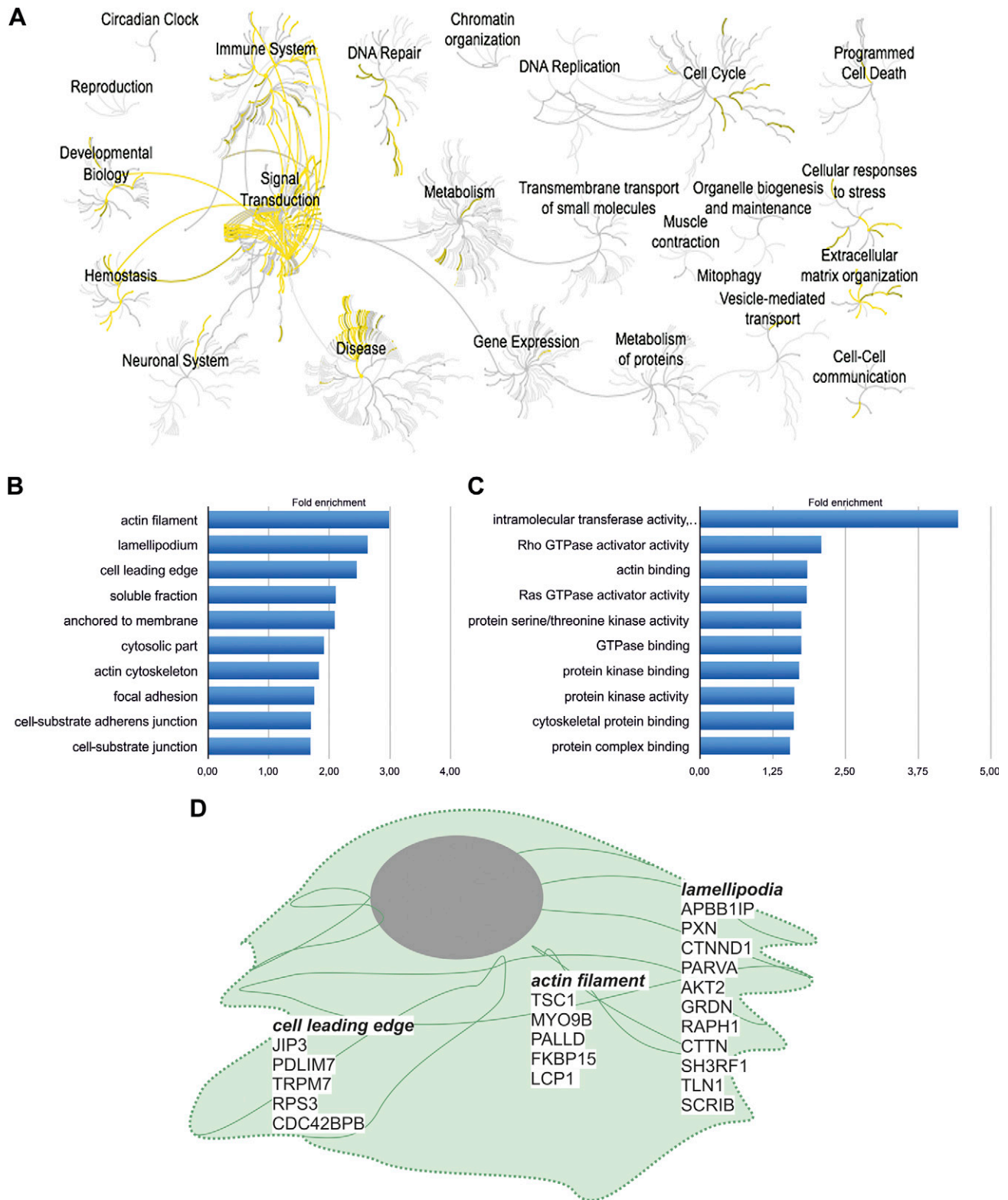


Figure 2. Signaling pathways over-represented among regulated phosphoproteins. *A*) Analysis demonstrates that proteins involved in signal transduction are predominant among increased phosphopeptides. *B*) A gene ontology functional classification regarding cellular components revealed that phosphopeptides related to actin filaments, lamellipodia, and cell leading edge were over-represented among increased phosphopeptides. *C*) A gene ontology functional classification revealed that phosphopeptides related to molecular functions, such as intramolecular transferase activity and Rho GTPase activator activity, were increased after AngII stimulation. *D*) Schematic representation of increased phosphoproteins associated with cellular components cell leading edge, actin filament, and lamellipodia, as defined by gene ontology terms.

TABLE 2. List of all actin-associated proteins from the study

Gene symbol	Median, all peptides	Peptide minimum	Peptide maximum
LCP1	4.01	0.92	7.09
PALLD	2.15	1.09	4.17
PHACTR4	1.26	0.47	3.62
MYLK	1.3	1.03	3.19
FKBP15	1.46	0.85	3.03
PLEC	0.98	0.56	2.99
MARCKS	1.22	0.74	2.26
VCL	1.62	1.43	2.15
FLNA	1.34	0.93	2.04
SNTB2	1.23	1.04	2.03
TNS1	1.42	0.78	1.97
PARVA	1.97	1.97	1.97
CYTSA	1.61	0.98	1.92
SSH2	1.61	1.09	1.88
MPRIP	1.03	0.81	1.87
LASP1	1.85	1.85	1.85
MN2	1.55	1.03	1.81
EHBP1	1.29	1.1	1.74
ADD1	1.25	1.06	1.7
FLNC	1.34	1.18	1.68
INF2	1.18	0.9	1.68
ARHGEF7	1.65	1.64	1.67
SPTBN1	1.06	0.42	1.63
MYO9B	1.36	0.99	1.61
FLNB	1.4	0.64	1.57
SPIRE1	1.56	1.56	1.56
BAIAP2L1	1.05	0.91	1.55
CAP1	1.35	1.08	1.54
CFL1	1.44	1.27	1.49
ANLN	1.29	1.21	1.49
EMD	1.48	1.48	1.48
SMTN	1.27	1.2	1.47
ACTN1	1.43	1.43	1.43
EPB41L1	0.99	0.79	1.41
MYH9	1.36	0.95	1.39
ADD3	1.22	0.96	1.38
PHACTR2	1.37	1.37	1.37
SNTA1	1.36	1.36	1.36
LIMA1	1.02	0.92	1.36
FLII	1.34	1.34	1.34
NAV2	1.14	0.81	1.3
LQGAP3	1.29	1.29	1.29
ANXA2	1.13	1	1.29
MACF1	1.13	1.08	1.29
DIAPH1	1.26	1.26	1.26
FMNL1	1.24	1.24	1.24
DIAPH3	1.22	1.22	1.22
EHBP	0.98	0.76	1.21
DST	0.88	0.78	1.19
ARPC5L	1.17	1.17	1.17
DBN1	1.08	0.89	1.17
ARHGEF6	1.15	1.15	1.15
AFAP1	1.06	1.03	1.14
EPB41L2	1.09	0.97	1.13
MYH10	1.13	1.13	1.13
LMO7	0.99	0.89	1.11
CYTSB	0.99	0.92	1.1
LIMCH1	1.05	0.89	1.09
CLMN	1.08	1.08	1.08
CALD1	1.07	1.07	1.07
EPB41L3	0.99	0.86	1.06
MICAL3	1.05	1.05	1.06

(continued)

TABLE 2. (continued)

Gene symbol	Median, all peptides	Peptide minimum	Peptide maximum
SYNE2	1.04	1.04	1.04
SPTAN1	1.03	1.03	1.03
SNTB1	1.01	0.99	1.03
ACTN4	1.03	1.03	1.03
MAPRE2	0.97	0.85	1.01
PPP1R9A	1.01	1.01	1.01
NEXN	0.98	0.95	1.01
SVIL	0.96	0.86	1.01
LRCH3	1	1	1
TMOD3	1	1	1
MICAL1	0.75	0.6	0.98
MICAL2	0.96	0.96	0.96
UTRN	0.96	0.96	0.96
SYNE1	0.89	0.89	0.89
MICAL1	0.8	0.74	0.87
LRCH1	0.8	0.8	0.8
SYNPO	0.8	0.8	0.8
SHROOM3	0.79	0.79	0.79
SYNPO2	0.76	0.75	0.76
WASF2	0.74	0.73	0.74
ABLIM1	0.65	0.65	0.65

phosphorylation, cells were treated with LPS, which resulted in a slight increase in phosphorylation.

AngII treatment, in addition to the activation of ERK and phosphorylation of LCP1 already shown in Supplemental Fig. 3, led to increased phosphorylation of RSK at Thr359. This phosphorylation of RSK and of ERK and LCP1 could be reduced by preincubation with the AT1R blocker losartan.

It has been demonstrated in breast cancer cell lines that ERK, RSK, PKA, and PKC are involved in the regulation of LCP1 phosphorylation at Ser5 (27, 39, 40); therefore, we investigated whether these kinases are also responsible for LCP1 phosphorylation in podocytes. Treatment with the specific RSK inhibitor, BID1870 (41), or the ERK inhibitor, U0126 (42), completely blocked AngII-induced LCP1 phosphorylation, which demonstrated that ERK and RSK are involved in LCP1 phosphorylation also in podocytes. The inhibitor, U0126, is an indirect ERK inhibitor and prevented AngII-induced ERK phosphorylation (Fig. 3A) *via* inhibition of the kinase MEK1/2, which usually phosphorylates and activates ERK (42). In contrast, the RSK inhibitor used in this study directly inhibited RSK kinase activity without influencing AngII-induced phosphorylation of RSK (Fig. 3A) (41).

In addition to phosphorylation *via* ERK and RSK, the PKA-mediated phosphorylation of LCP1—previously shown in breast cancer cells (39)—could be confirmed in podocytes. Preincubation with the PKA-specific inhibitor, RP-8-Br-cAMP (43), diminished LCP1 phosphorylation, whereas RSK phosphorylation was preserved after treatment (Fig. 3B). This result suggests that LCP1 Ser5 is not exclusively phosphorylated by RSK but also in parallel by PKA.

Similarly, inhibition of PKC with the pan-PKC inhibitor, GF109203X (44), blocked AngII-induced LCP1 phosphorylation (Fig. 3C). It also influenced RSK phosphorylation

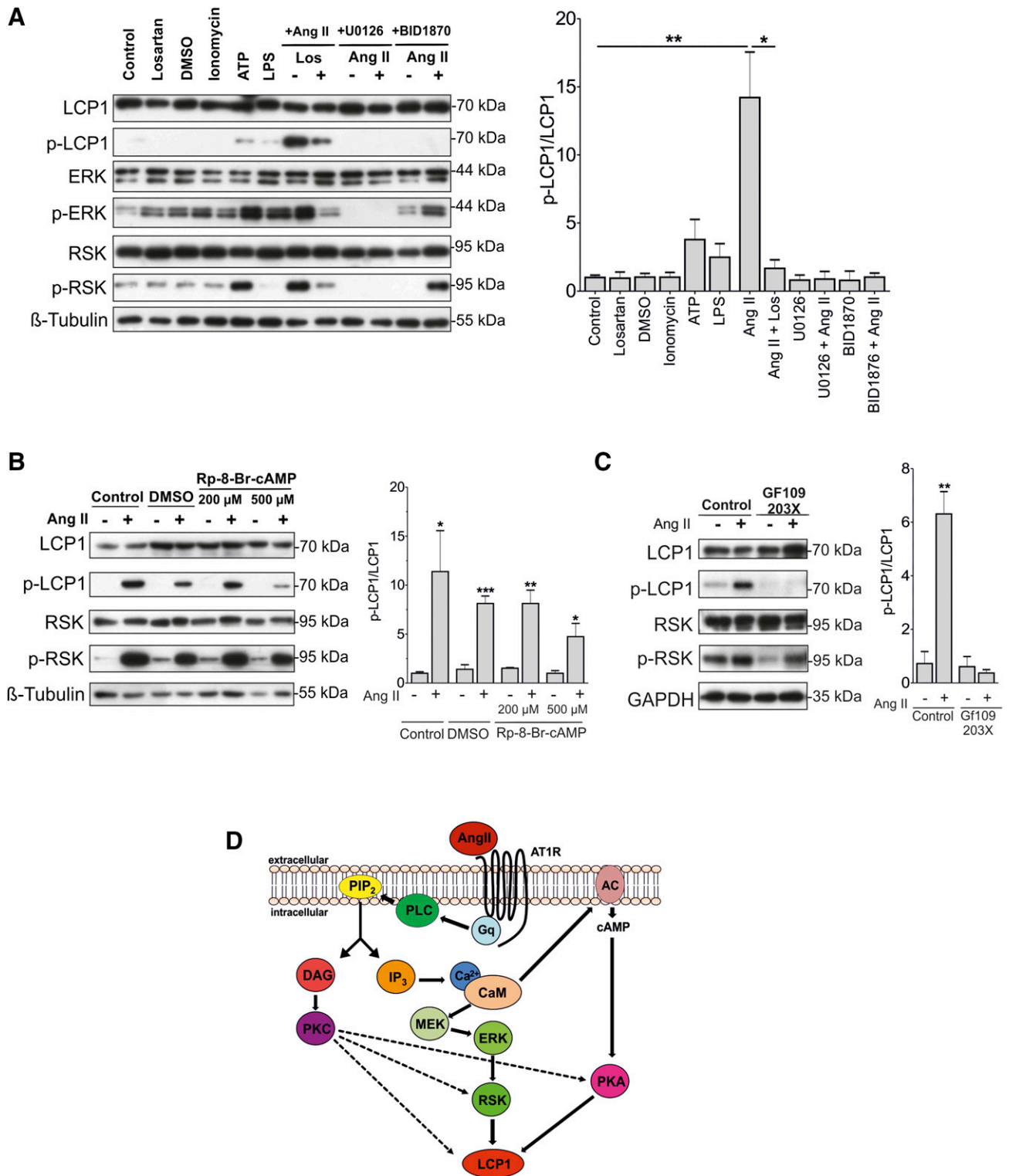


Figure 3. Phosphorylation of LCP1 is AngII dependent and can occur *via* ERK, RSK, PKA, and PKC kinases. For a more precise examination of AngII-dependent signaling events that result in LCP1 phosphorylation, different kinase inhibitors were used. In addition, the induction of LCP1 phosphorylation by general calcium increase (ATP, ionomycin) or podocyte damage (LPS) was tested. **A)** Representative Western blot results from podocytes that were treated with AngII (100 nM, 15 min), ionomycin (500 nM, 5 min), ATP (1 μ M, 5 min), or LPS (1 mM, 24 h) (left). Where indicated, cells were preincubated with AT1R blocker (Los; 10 μ M, 2 h), RSK inhibitor BID1870 (10 μ M, 4 h), or ERK inhibitor U0126 (10 μ M, 2 h). Ratio between phosphorylated and total amount of LCP1 from 4 independent experiments (right). **B)** Representative Western blot from podocytes that were treated with AngII (100 nM, 15 min) (left). Preincubation with PKA-specific inhibitor Rp-8-Br-cAMP in higher concentration diminishes AngII-induced LCP1 phosphorylation. Ratio between phosphorylated and total amount of LCP1 from 4 independent experiments (right). **C)** Representative Western blot results from podocytes that were treated with AngII (100 nM, 15 min) (left). Preincubation with the (continued on next page)

as treatment with GF109203X reduced the p-RSK signal; however, treatment with AngII still activates RSK (phosphorylation of RSK), which indicated an RSK-independent contribution of PKC to LCP1 phosphorylation.

In summary, our data indicate that AngII-induced LCP1 phosphorylation in podocytes can occur in parallel *via* activation of ERK and subsequently RSK or *via* an AngII-induced PKA activation or *via* PKC activation, directly or indirectly *via* RSK or PKA (Fig. 3D).

Intracellular localization of LCP1 changes after AngII stimulation

Immunofluorescent staining of endogenous LCP1 in podocytes demonstrated that LCP1 colocalized, in part, with actin, particularly in needle-like cell–cell contacts (Fig. 4A, top). LCP1 staining in such extensions was observed in a previous study and the structures were identified as filopodia (45). Indeed, we also observed LCP1 and actin-stained filopodia forming cell–cell contacts in podocytes. During AngII treatment, LCP1 and actin redistributed to cell borders (Fig. 4A, bottom). Furthermore, the morphology of cell–cell contact sites changed: the number of needle-like structures seemed to decrease after AngII stimulation and, instead, cell contact sites seemed to be broadened, in parts overlapping. This observation was confirmed in experiments with cells that were grown to confluence. These cells were too dense to visualize filopodia but AngII stimulation induced membrane ruffling; cells seemed to enlarge and grow out of the cell assembly, forming lamellipodia (Fig. 4B). To quantify the effect of membrane ruffling, we counted the cells with ruffled membranes with or without AngII treatment and confirmed that nearly all cells reacted to AngII stimulation with membrane ruffling (Fig. 4C).

As such actin-based changes at the plasma membrane as filopodia or lamellipodia formation are often initial steps for cell–cell contact formation, we applied a cell aggregation assay to investigate whether AngII stimulation influences cell–cell aggregation of podocytes. For this assay, cells were cultured in suspension with and without AngII. Indeed, our experiments revealed significantly increased AngII-dependent cell clustering (Fig. 4D), which fits to previous observations made by Janji *et al.* (27) that showed that LCP1 phosphorylation influences the cell–cell contact formation in HEK293T cells.

LCP1 phosphorylation influences cell–cell contacts and filopodia formation

It has been previously shown that phosphorylation of LCP1 at Ser5 promotes the targeting of LCP1 to actin assembly sites (27, 40). To address this, we visualized endogenously

phosphorylated LCP1 (p-Ser5–LCP1) in podocytes. Staining with a highly specific Ab (27) demonstrated that p-Ser5–LCP1 was predominantly localized at the cell periphery and in the filopodia; however, neither the increase in the pLCP1 signal, nor a redistribution of pLCP1 could be shown convincingly in this immunofluorescence experiment (Supplemental Fig. 4). Therefore, we cloned LCP1 constructs that were tagged with RFP to characterize the phosphorylation-dependent change of LCP1 distribution in more detail. In addition to LCP1-WT, we cloned a LCP1 mutant (LCP1-S5E) that mimics phosphorylation by exchange of Ser5 with glutamic acid as well as a non-phosphorylatable mutant (LCP1 S5A) by exchange of Ser5 with alanine. Expression of the constructs and AngII-induced phosphorylation of RFP-tagged LCP1—similar to endogenous LCP1—was verified in HEK293T cells (Supplemental Fig. 5).

In transiently transfected podocytes, RFP-LCP1-WT was mainly localized in the cytoplasm, colocalizing, in part, with actin. In less dense cell layers, RFP-LCP1-WT colocalized with actin in the filopodia in parallel to our observations of endogenous LCP1 (Figs. 4A and 5A). In cells that were transfected with the phosphomimicking mutant, S5E, we also observed LCP1-stained filopodia (Fig. 5A); however, the number of filopodia of cells that were transfected with nonphosphorylatable mutant (S5A) was reduced (Fig. 5A). To confirm this observation, we evaluated the amount and length, preferably of single cells that were transfected with the three LCP1 constructs or with control plasmid (Fig. 5B). In cells that were transfected with nonphosphorylatable S5A variant, filopodia number or length did not differ from mock-transfected cells (Fig. 5C). In contrast, transfection with the LCP1-S5E variant and WT increases filopodia formation in both number and length. This indicates that LCP1 phosphorylation is crucial for filopodia formation. On the basis of these results, we conclude that AngII-induced LCP1 phosphorylation influences cell–cell contact formation.

AngII-induced lamellipodia formation is independent of LCP1 phosphorylation

AngII-induced LCP1 redistribution was studied in more detail in live cell imaging studies of podocytes that were transiently transfected with RFP-tagged LCP1-WT (Fig. 6A). Addition of water did not alter the cell shape (Fig. 6A, line 1); however, treatment with AngII (Fig. 6A, line 2) induced membrane ruffling and directed lamellipodia outgrowth at the cell periphery. Lamellipodia outgrowth that resulted in an increase in RFP-signals at the cell periphery was used to quantify the AngII effect, termed cell area enlargement (Supplemental Video 1; LCP1 WT + AngII). Ruffling activity

pan-PKC inhibitor GF109203X completely blocked AngII-induced phosphorylation of LCP1. Ratio between phosphorylated and total amount of LCP1 from 3 independent experiments (right). D) Schematic representation of the regulation of LCP1 phosphorylation downstream of AngII and AT1R in podocytes. Dotted lines from PKC include the possibility that LCP1 is phosphorylated by PKC directly or mediated by PKA or RSK. Data are means \pm SD, Student's *t* test. **P* < 0.05, ***P* < 0.01, ****P* < 0.001.

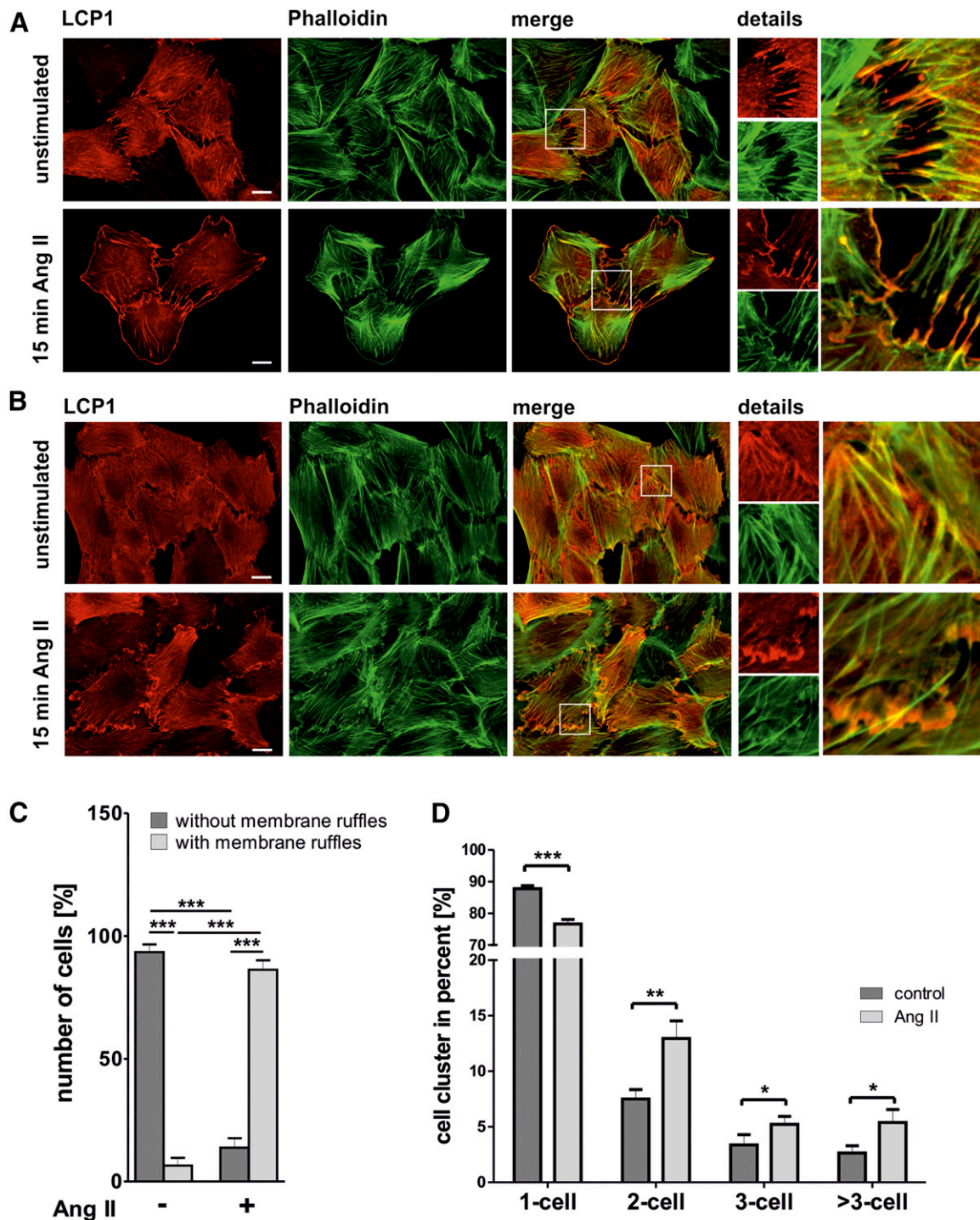


Figure 4. AngII triggers the redistribution of LCP1 localization. *A*) Immunofluorescent staining of endogenous LCP1 (red) and actin (phalloidin, green) before and 15 min after stimulation with AngII (100 nM) indicates an AngII-dependent redistribution of LCP1 to the cell margins in podocytes. Details illustrate the needle-like cell–cell contacts in unstimulated cells, which seemed to be broadened, in part overlapping, after AngII stimulation. *B*) AngII treatment leads to the formation of membrane ruffles at cell margins, especially remarkable in LCP1 staining. *C*) Quantification of cells with ruffled membranes evaluated from untreated cells ($n = 215$) and cells after AngII treatment ($n = 169$; 100 nM, 15 min). *D*) Cells were cultured in suspension with and without AngII (100 nM). Single cells and cell clusters of treated and control cells were calculated after 30 min incubation. Scale bars, 20 μm . Data are means \pm sd, Student's *t* test. * $P < 0.05$, ** $P < 0.01$, *** $P < 0.001$.

and cell area enlargement persisted for the entire observation period of 15 min. This AngII-induced LCP1 redistribution could be blocked by preincubation with the AT1R-antagonist, losartan (Fig. 6A, line 3); however, preincubation with RSK inhibitor, which completely inhibited

AngII-induced LCP1 phosphorylation at Ser5 (Fig. 3A), had no influence on AngII-induced cell area enlargement (Fig. 6A, line 4). This suggested that cell area enlargement was not regulated by Ser5 phosphorylation. Similar effects on cell area enlargement were observed in cells that were

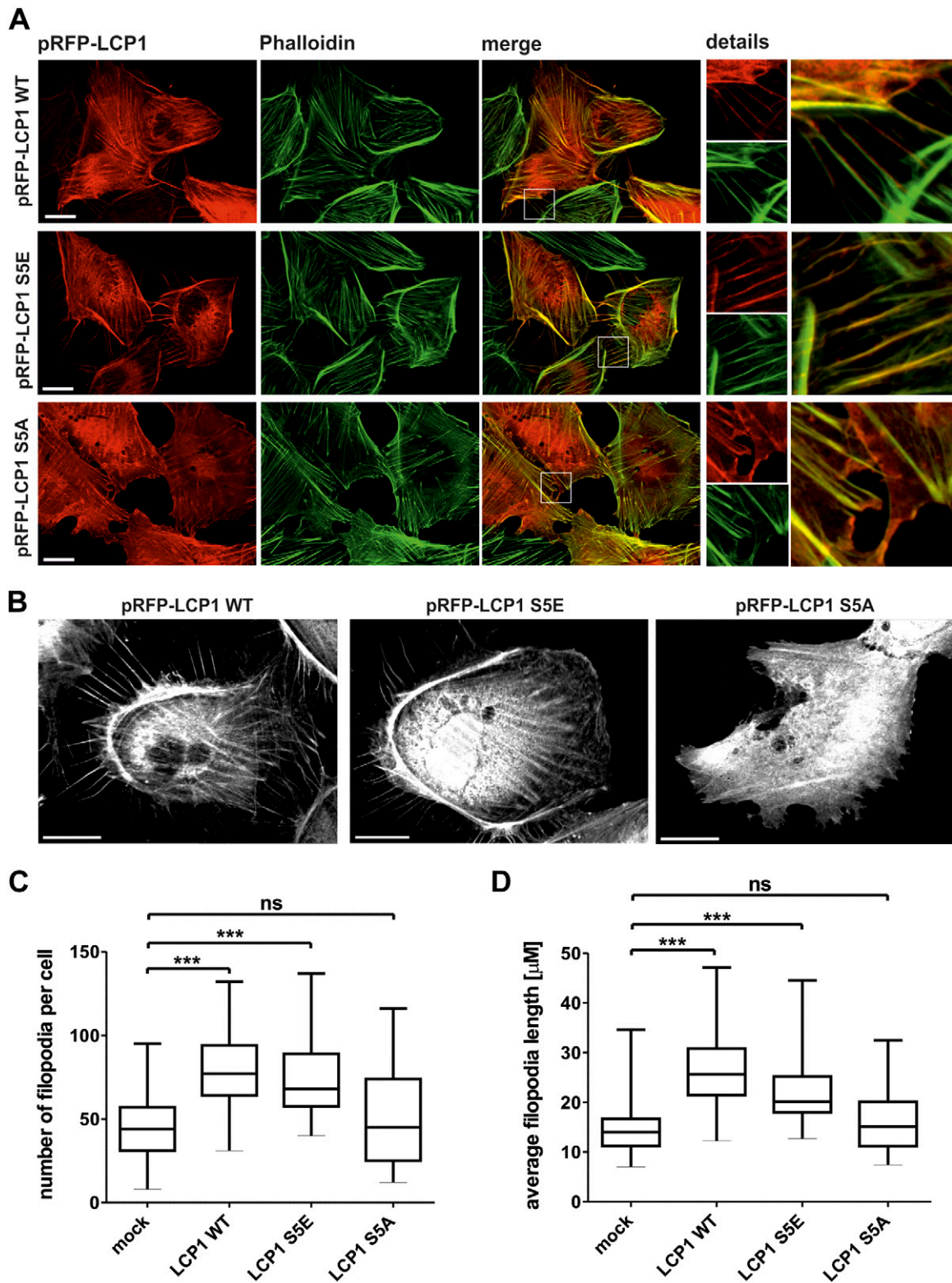


Figure 5. LCP1 phosphorylation influences filopodia formation. Podocytes were transfected with fluorescence-labeled (RFP) LCP1-WT, a LCP1 mutant (LCP1-S5E) that mimics phosphorylation and a nonphosphorylatable mutant (LCP1-S5A). *A*) Immunofluorescence images of podocytes that were transfected with 3 LCP1 mutants also stained against actin (phalloidin, green). Details show differences in cell-cell contact sites dependent on the transfected LCP1 mutant. *B*) Representative cells of podocytes that were transfected with 3 LCP1 mutants showing differences in filopodia number and length. *C, D*) Quantification of the number and length of filopodia in podocytes that were transfected with 3 LCP1 mutants compared with control-transfected cells ($n \geq 3$, means \pm sd, Student's *t* test). Scale bars, 20 μ m. * $P < 0.05$, ** $P < 0.01$, *** $P < 0.001$.

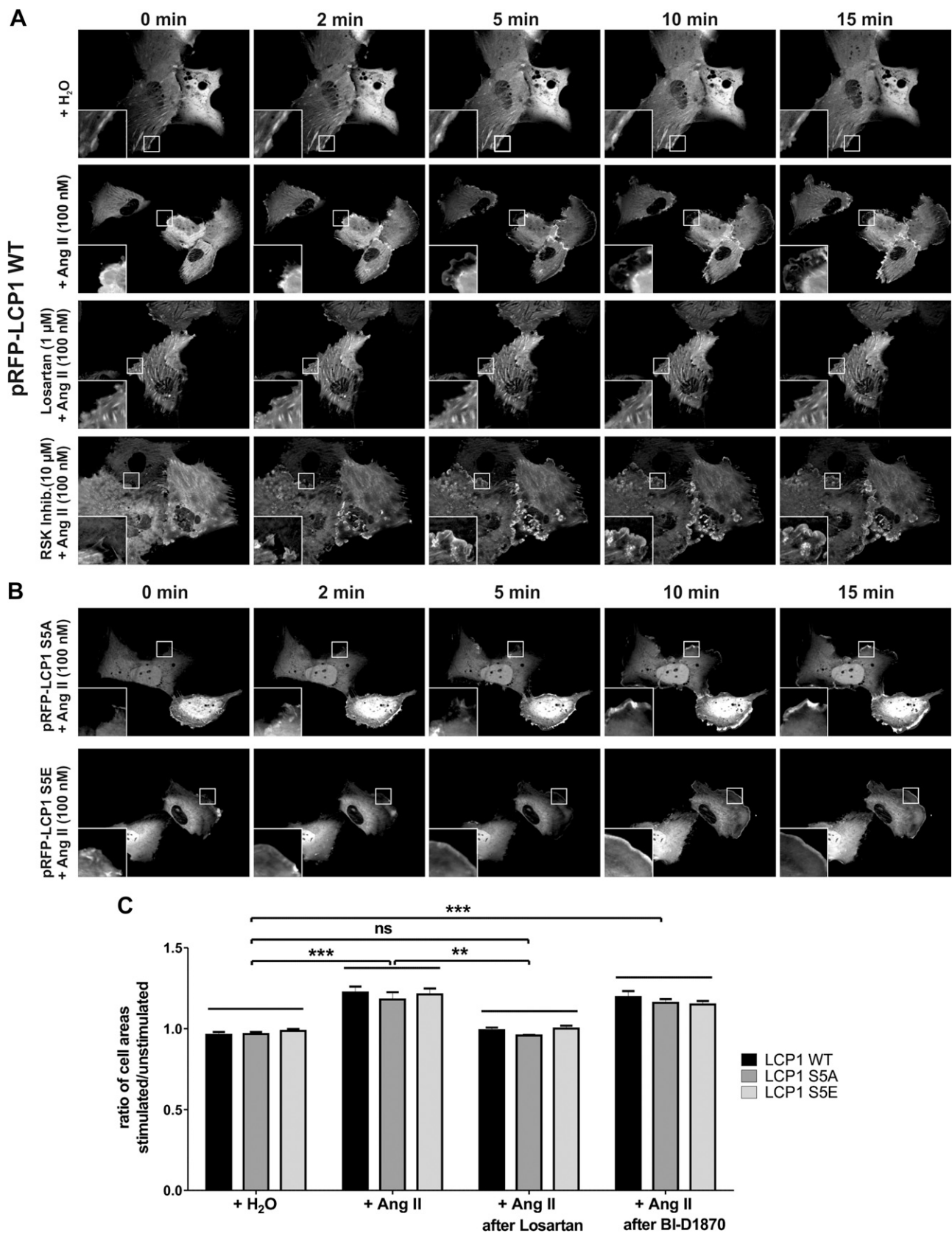


Figure 6. AngII-induced LCP1 redistribution and membrane ruffling is independent of LCP1 phosphorylation. *A*) Representative live cell imaging experiment of podocytes that were transiently transfected with fluorescent RFP-LCP1-WT. Stimulation of cells was performed in line 1 by adding water as control, and in lines 2–4 by adding AngII (100 nM). For original movie of line 2 see the Supplemental Data. Cells in line 3 were incubated before stimulation with AT1R blocker losartan (Los; 10 μ M, 2 h), and cells in line 4 were incubated with the RSK inhibitor BID1870 (10 μ M, 3 h). The image labeled 0 min was taken before stimulation, (continued on next page)

transfected with LCP1-S5A and LCP1-S5E mutants (Fig. 6B) which confirmed that this effect is independent of phosphorylation.

To quantify cell area enlargement, we measured the area of cells that were transfected with RFP-tagged LCP1 mutants before AngII treatment and 15 min after AngII stimulation. Changes in these areas were summarized as the ratio of cell areas of stimulated *vs.* unstimulated cells (Fig. 6C). With this ratio as readout, an objective quantification of cell enlargement was possible, which allowed a comparison of different experiments. Here, our evaluation confirmed an AngII-induced cell enlargement in podocytes, which is independent of LCP1 phosphorylation.

Ca²⁺-binding EF hand motifs of LCP1 are crucial for AngII-induced lamellipodia formation

In addition to the activation of several kinases that leads to the phosphorylation of various proteins, extracellular stimulation of AT1R with AngII increases the level of intracellular calcium (10, 11). LCP1 has two EF hand motifs near the N-terminus that negatively regulate the actin bundling activity of LCP1 by calcium binding (46, 47). Therefore, we hypothesized that membrane ruffling and lamellipodia formation after AngII stimulation could also be regulated by the Ca²⁺ binding ability of LCP1 and cloned two LCP1 deletion mutants, one of which lacks the complete N-terminus (LCP1_minus EF) and the other which lacks the EF hand motifs (LCP1_phospho_minus EF; Fig. 7A). The effects of these deletions were examined in live cell imaging studies (Fig. 7B). We again used cell area enlargement as readout. In contrast to LCP1-WT, AngII stimulation did not lead to cell area enlargement in cells that expressed the deletion mutants, despite LCP1 redistribution and membrane ruffling. The presence or absence of the phosphosite made no difference. The same effect was achieved with LCP1-WT-transfected cells when intracellular and extracellular Ca²⁺ concentrations were reduced. Quantification of cell enlargement confirmed this observation (Fig. 7C). These results indicate that AngII-induced lamellipodia formation in LCP1-transfected podocytes is mainly regulated by the increase in intracellular Ca²⁺ concentration. Additional experiments demonstrate that AngII can also regulate T-plastin in a calcium-dependent manner (Supplemental Fig. 6).

However, our data strongly indicate that LCP1—in contrast to other members of the plastin family—is regulated by 2 different AngII-dependent mechanisms. First, *via* activation of various serine/threonine kinases, and second, *via* increased Ca²⁺-influx, which suggests that the regulation of LCP1 is more complex than that

of other members of the plastin family—I-plastin and T-plastin—that lack the phosphorylation site at the N-terminus.

Taken together, our data indicate that AngII-dependent phosphorylation of actin-associated proteins occurs *via* ERK, RSK, PKA, and PKC kinases. Focusing on LCP1, our study highlights that AngII can influence protein activity by different effects—Ca influx and activation of kinases—indicating that AngII influences cytoskeletal dynamics in podocytes within a complex and, presumably, finely tuned signaling network.

DISCUSSION

The fate and function of podocytes are based on their complex architecture and, in particular, on the integrity of their actin cytoskeleton (48). It has been suggested that changes in the actin cytoskeleton and intracellular Ca²⁺ play a major role in the morphogenesis and pathology of podocytes (49). Global reorganization of actin and, ultimately, foot process effacement are hallmarks of glomerular diseases. AngII directly affects the actin cytoskeleton of podocytes, and, in the long-term, AngII and increased RAAS contribute to the progression of glomerular injury (6). AngII depolarizes glomerular cells by leading to an increase of cytosolic calcium concentration and, in podocytes, by activation of a calcium-dependent Cl⁻ conductance (50). Moreover, AngII induces a shift of the podocyte phenotype from a dynamically stable type to an adaptively migratory type. This is conferred among others *via* the influence on the actin cytoskeleton (12).

Glomerular diseases that are caused by diabetes, hypertension, or immunologic processes represent the major cause of chronic kidney disease, which affects more than 5% of the population worldwide. Therapeutic inhibition of AngII signaling *via* administration of AT1R blocker and angiotensin-converting enzyme inhibitors lowers mortality and may delay disease progression and, thus, is recommended for most patients with chronic kidney disease. Additional understanding of the molecular action of AngII in podocytes will lead to the identification of novel treatment strategies.

The aim of our current study was to obtain greater insight into intracellular AngII/AT1R pathway-dependent phosphorylation and, especially, to identify which kinases contribute to the signal transduction processes. Therefore, we employed an SILAC-based approach and analyzed changes in the phosphoproteome in podocytes after short-term treatment with AngII. With this technique, we identified 6323 independent phosphopeptides that corresponded to 2081 different proteins. More than three fourths of proteins identified in our screen have been previously found in a non-phospho-specific characterization of the mouse

whereas the other pictures were obtained at the indicated time points after stimulation. *B*) Representative live cell imaging experiment of podocytes that were transiently transfected with fluorescent RFP-LCP1-S5A or -S5E stimulated with AngII (100 nM). The image labeled 0 min was taken before stimulation, whereas the other pictures were obtained at the indicated time points after stimulation. *C*) Quantification of cell enlargement after stimulation from live cell experiments using ImageJ. RFP-labeled cell areas at time point 0 min were determined as unstimulated values and at time point 15 min as stimulated values. The ratio of cell areas is shown ($n \geq 3$, mean \pm SD, Student's *t* test). * $P < 0.05$, ** $P < 0.01$, *** $P < 0.001$.

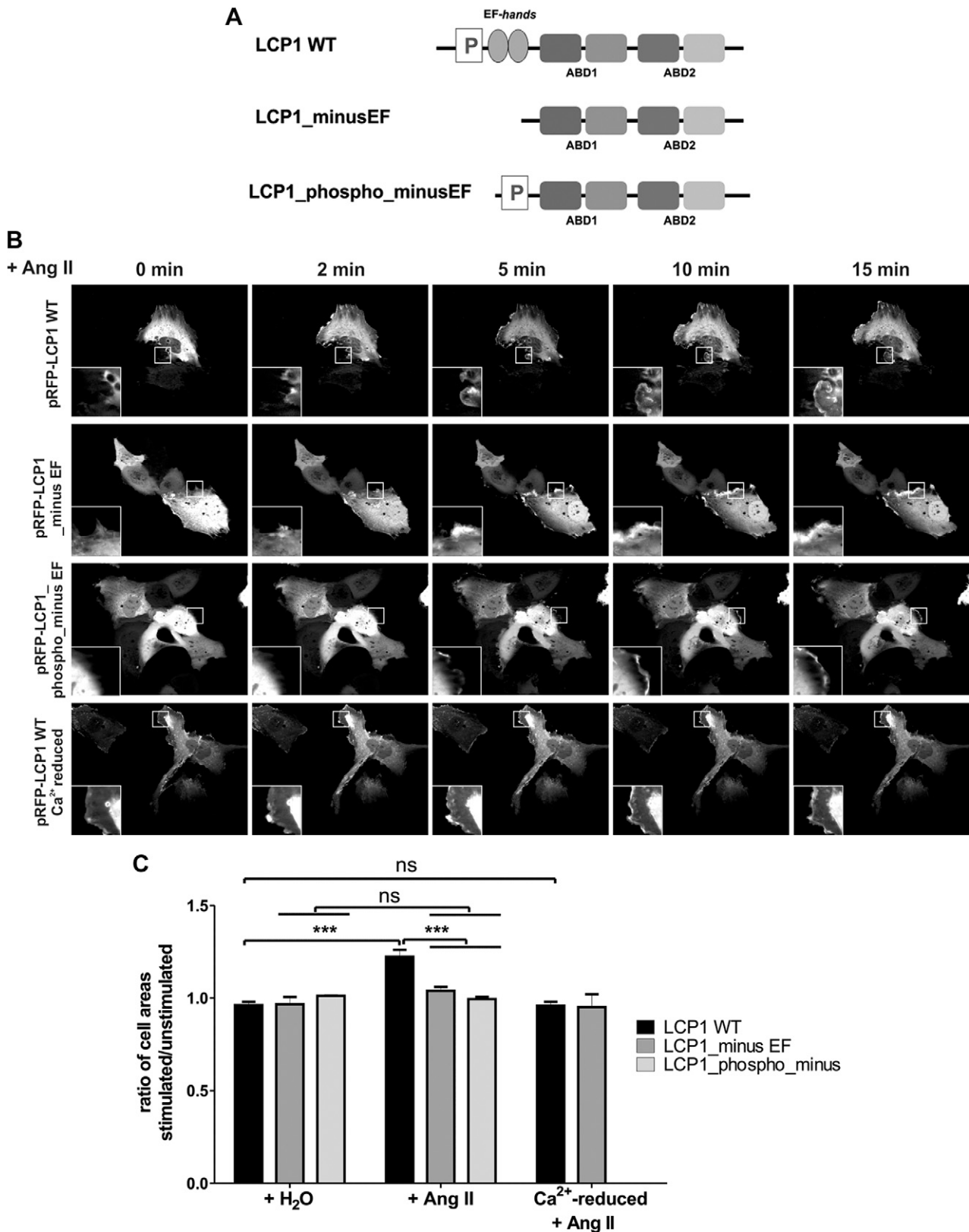


Figure 7. AngII-induced membrane ruffling is predominantly Ca²⁺ dependent. *A*) Schematic overview of LCP1 deletion mutants without EF-binding sites [actin-binding domain (ABD)]. *B*) Representative live cell imaging experiment of podocytes that were transiently transfected with fluorescent RFP-LCP1-WT (lines 1 and 4) or the 2 deletion mutants as indicated (lines 2 and 3). For the experiment in line 4, intracellular and extracellular Ca²⁺ concentration was reduced. Stimulation of cells was performed by adding AngII (100 nM). The image labeled “0 min” was taken before stimulation, whereas the other pictures were obtained at the indicated time points after stimulation. *C*) Quantification of cell enlargement after stimulation from live cell experiments. RFP-labeled cell areas at time point 0 min were determined as unstimulated values and at time point 15 min as stimulated values using ImageJ. The ratio of cell areas is shown ($n \geq 3$, means \pm SD, Student's t test). * $P < 0.05$, ** $P < 0.01$, *** $P < 0.001$.

podocyte proteome (34), which validated the outcome of this SILAC approach. Of interest, one fourth of proteins identified in our approach are new and had not been identified in the mouse podocyte proteome, likely as a result of the phospho-enrichment of proteins of our podocyte cell line.

One hundred twenty-one of the phosphoproteins that were increased in our study were also regulated in a previous study with AT1R-overexpressing HEK293 cells, which suggests that the 323 novel proteins identified in this study could be podocyte specific (35).

A large number of identified phosphopeptides correspond to extracellular matrix proteins (Table 1). Expression of these proteins in the human kidney and their phosphorylation at extracellular residues has also been observed in prior studies (51–53); however, the significance of their increased phosphorylation as observed in cell lysates is unknown and should be addressed in future studies.

Our data demonstrate a predominant phosphorylation of actin filament-associated proteins, which is in accordance with other studies in HEK293 cells (22, 35, 54) and indicates that AngII-induced phosphomodification of actin cytoskeleton-associated proteins could be a common feature in different cell types (Fig. 2D).

Although AngII-induced regulation of the cytoskeleton has been previously implicated in podocyte pathology, the exact mechanisms of cytoskeletal rearrangement upon AngII exposure are elusive. Podocytes are unique cells at the glomerular slit diaphragm. To fulfill their function as a filter, they require an intact and flexible actin cytoskeleton. On this basis, the strong AngII-induced increase in phosphorylation of actin-associated protein LCP1 at Ser5 (factor 4.77; Table 1) stood out among the most enriched phosphopeptides in our screen. LCP1 belongs to the α -actinin protein family and is involved in actin cross-linking and actin bundling. Although this protein was found in several other proteomics studies (<https://hpcwebapps.cit.nih.gov/ESBL/Database/PodocyteProteome/index.html>), to our knowledge, ours is the first study to focus on the AngII-dependent phosphorylation of LCP1, and we have demonstrated LCP1 protein expression and its phosphorylation upon AngII treatment on the protein level in podocytes. To assess whether AngII-induced LCP1 phosphorylation was a consequence of AngII-induced intracellular Ca^{2+} increase, we treated podocytes with the ionophore ionomycin; however, ionomycin did not lead to increased LCP1 Ser5 phosphorylation, which suggests that a mere increase in intracellular Ca^{2+} is not sufficient for LCP1 phosphorylation. In contrast, treatment of podocytes with ATP resulted in LCP1 phosphorylation, which is similar to the effect of AngII. Unlike ionomycin, AngII and ATP ligands signal *via* activation of GPCRs that ensure well-balanced local modulation of the intracellular Ca^{2+} concentration. In addition to this, GPCR activation triggers multiple signal-transduction cascades, which suggests that kinases that are downstream of AngII/AT1R lead to phosphorylation of LCP1.

Similar to that in breast cancer cells (39), LCP1 phosphorylation in podocytes was influenced by ERK, RSK, PKA, and PKC activity (Fig. 3), which suggests that LCP1 phosphorylation by these kinases is not limited to certain cell types and is also present in podocytes.

Immunofluorescence experiments demonstrated an AngII-dependent LCP1 targeting to the cell margins (Fig. 4). Moreover, membrane ruffling and alterations of cell-cell contacts correlated with an increased cell-cell clustering after AngII stimulation. A correlation of LCP1 redistribution, membrane ruffling, and actin binding has previously been observed by other groups. For example, treatment of LCP1 MCF-7 breast carcinoma cells with phorbol 12-myristate 13-acetate, which is a potent activator of conventional and novel PKC family members (55), also led to increased LCP1 phosphorylation, LCP1 relocalization, and membrane ruffling (40). Furthermore, phosphomimicking LCP1-S5E was observed to accumulate in actin-rich regions in monkey kidney epithelial cells (Vero cells) (27). Ser5 phosphorylation has been described to modulate the actin dynamics in focal adhesions, which suggests that LCP1 redistribution to *de novo* assembled actin-rich structures depends on phosphorylation (40). However, the authors admitted that nonphosphorylatable LCP1-S5A also shifted to cell margins after treatment with phorbol 12-myristate 13-acetate, but to a lesser degree (40). This result is in line with our live cell experiments. Treatment of podocytes with an RSK inhibitor, which effectively inhibited LCP1 phosphorylation (Fig. 3A), could not suppress membrane ruffling, lamellipodia formation, and cell area enlargement after AngII stimulation in LCP1-WT-, LCP1-S5A-, or LCP1-S5E-transfected cells (Fig. 6). This indicates that membrane ruffling and lamellipodia formation do not strictly require LCP1 phosphorylation.

It is known that increased calcium concentrations negatively regulate the actin-bundling activity of LCP1 (46). It has been recently shown that LCP1 contains a switch helix structure that, in the presence of calcium, tightly binds to EF-hand motifs (47). This conformational change reduces the actin-bundling capacity of LCP1 in the presence of calcium. Our results suggest that calcium-dependent regulation of actin bundling is crucial for lamellipodia formation as the expression of the deletion mutants without calcium binding capacity or a reduction in calcium concentration prevented a successful lamellipodia formation with cell area enlargement (Fig. 7).

Otherwise we could show that LCP1 phosphorylation influences filopodia formation (Fig. 5) as in contrast to podocytes expressing the nonphosphorylatable mutant of LCP1 (LCP1-S5A) podocytes expressing the phosphorylatable (LCP1-WT) or phosphomimicking form (LCP1-S5E) of LCP1 formed an increased number of prolonged filopodia. Of interest, a group investigating the influence of recombinant LCP1 single-domain Abs that bind to different regions of LCP1 also observed an influence on filopodia formation comparable to our results (45). One of the examined Abs inhibited the formation of long filopodia. This Ab bound to the second actin-binding domain of LCP1, which led to the conclusion that the actin-bundling activity of LCP1 plays a fundamental role in filopodia integrity. Actin bundling activity is influenced by LCP1 phosphorylation (40). In general, actin-bundling proteins, among other plastins, are involved in the assembly of filopodia (56). An accumulation of LCP1 in focal adhesions and membrane protrusions has been described previously (27, 40). It could be demonstrated that phosphorylation of

LCP1 increases its association rate to actin in focal adhesions, thereby decreasing the dissociation rate of F-actin (40). In epithelial cells, filopodia are important for cell–cell contacts and cell migration (56); therefore, increased cell clustering and altered cell–cell contact formation in podocytes after AngII stimulation might be connected with changed filopodia formation as a result of LCP1 phosphorylation.

From all these results, it is tempting to speculate that both the phosphorylation of LCP1 and calcium binding influence the actin-bundling activity of LCP1, but in different ways and upon different triggers. Consequently, AngII stimulation has diverse and, in part, competitive effects on LCP1 activity, the effect of membrane ruffling and lamellipodia formation obviously overlaying the effect of filopodia formation.

Expression of LCP1 in podocytes *in vivo* has also been found in other proteomic studies. LCP1 expression is not over-represented in podocytes and seemed to be low (57, 58); however, a low expression level does not exclude an important role in the regulation or modulation of AngII-dependent actin cytoskeleton rearrangements in podocytes. In this context, it is of special interest that podocytes not only express LCP but also T-plastin; therefore, it will be interesting to investigate whether the expression of both plastins and/or the phosphorylation of LCP1 is increased during podocyte injury.

Considering the importance of the intact actin cytoskeleton, AngII-dependent changes in the phosphorylation of LCP1 or other actin-associated proteins, such as palladin, that facilitates G- and F-actin binding and the targeting of actin to specific foci (59) might contribute to podocyte viability or damage (Table 1).

Taken together, our study highlights the relevance of AngII-induced phosphorylation of actin-associated proteins and, thus, the regulation of actin dynamics in podocytes. The main phosphorylation cascades that are activated by AngII seem to be conserved, but apparently AngII signaling in podocytes is complemented by podocyte-specific signal transduction. LCP1 might act as a signal-integrating molecule and coregulator of actin dynamics upon different GPCR-dependent—in this case, AngII/AT1R—signaling cascades. Although additional studies are needed, the development of drugs that target the cytoskeletal turnover of actin-modulating proteins would be a promising approach for the treatment of diseases of the podocyte. FJ

ACKNOWLEDGMENTS

This work was supported by grants from the German Research Foundation (DFG; Grants PA 483/16-1 and BU 1214/4-1). The authors declare no conflicts of interest.

AUTHOR CONTRIBUTIONS

L. K. Schenk, D. Wolters, T. Weide, H. Pavenstädt, and B. Vollenbröcker designed research; L. K. Schenk and B. Vollenbröcker analyzed data; L. K. Schenk, A. Möller-Kerutt, D. Wolters, R. Klosowski, and B. Vollenbröcker

performed research; L. K. Schenk and B. Vollenbröcker wrote the paper; E. Schaffner-Reckinger contributed a novel antibody; and all authors revised the final version of the manuscript.

REFERENCES

1. Scott, R. P., and Quaggin, S. E. (2015) Review series: the cell biology of renal filtration. *J. Cell Biol.* **209**, 199–210
2. Fukuda, A., Wickman, L. T., Venkatarreddy, M. P., Sato, Y., Chowdhury, M. A., Wang, S. Q., Shedden, K. A., Dysko, R. C., Wiggins, J. E., and Wiggins, R. C. (2012) Angiotensin II-dependent persistent podocyte loss from destabilized glomeruli causes progression of end stage kidney disease. *Kidney Int.* **81**, 40–55
3. Wennmann, D. O., Hsu, H. H., and Pavenstädt, H. (2012) The renin-angiotensin-aldosterone system in podocytes. *Semin. Nephrol.* **32**, 377–384
4. Schweda, F. (2015) Salt feedback on the renin-angiotensin-aldosterone system. *Pflugers Arch.* **467**, 565–576
5. Dworkin, L. D., Ichikawa, I., and Brenner, B. M. (1983) Hormonal modulation of glomerular function. *Am. J. Physiol.* **244**, F95–F104
6. Remuzzi, G., Perico, N., Macia, M., and Ruggenenti, P. (2005) The role of renin-angiotensin-aldosterone system in the progression of chronic kidney disease. *Kidney Int. Suppl.* **2005**, S57–S65
7. Ruster, C., and Wolf, G. (2011) Angiotensin II as a morphogenic cytokine stimulating renal fibrogenesis. *J. Am. Soc. Nephrol.* **22**, 1189–1199
8. Kobori, H., Mori, H., Masaki, T., and Nishiyama, A. (2013) Angiotensin II blockade and renal protection. *Curr. Pharm. Des.* **19**, 3033–3042
9. Xie, X., Liu, Y., Perkovic, V., Li, X., Ninomiya, T., Hou, W., Zhao, N., Liu, L., Lv, J., Zhang, H., and Wang, H. (2016) Renin-angiotensin system inhibitors and kidney and cardiovascular outcomes in patients with CKD: a Bayesian network meta-analysis of randomized clinical trials. *Am. J. Kidney Dis.* **67**, 728–741
10. Eguchi, S., Frank, G. D., Mifune, M., and Inagami, T. (2003) Metalloprotease-dependent ErbB ligand shedding in mediating EGFR transactivation and vascular remodelling. *Biochem. Soc. Trans.* **31**, 1198–1202
11. Suzuki, H., Motley, E. D., Frank, G. D., Utsunomiya, H., and Eguchi, S. (2005) Recent progress in signal transduction research of the angiotensin II type-1 receptor: protein kinases, vascular dysfunction and structural requirement. *Curr. Med. Chem. Cardiovasc. Hematol. Agents* **3**, 305–322
12. Hsu, H. H., Hoffmann, S., Endlich, N., Velic, A., Schwab, A., Weide, T., Schlatter, E., and Pavenstädt, H. (2008) Mechanisms of angiotensin II signaling on cytoskeleton of podocytes. *J. Mol. Med. (Berl.)* **86**, 1379–1394
13. Morley, S. C. (2013) The actin-bundling protein L-plastin supports T-cell motility and activation. *Immunol. Rev.* **256**, 48–62
14. Wennmann, D. O., Vollenbröcker, B., Eckart, A. K., Bonse, J., Erdmann, F., Wolters, D. A., Schenk, L. K., Schulze, U., Kremerskothen, J., Weide, T., and Pavenstädt, H. (2014) The Hippo pathway is controlled by angiotensin II signaling and its reactivation induces apoptosis in podocytes. *Cell Death Dis.* **5**, e1519
15. Schulze, U., Vollenbröcker, B., Braun, D. A., Van Le, T., Granada, D., Kremerskothen, J., Fränzel, B., Klosowski, R., Barth, J., Fufezan, C., Wolters, D. A., Pavenstädt, H., and Weide, T. (2014) The Vac14 interaction network is linked to regulators of the endolysosomal and autophagic pathway. *Mol. Cell. Proteomics* **13**, 1397–1411
16. Tchapyjnikov, D., Li, Y., Pisitkun, T., Hoffert, J. D., Yu, M. J., and Knepper, M. A. (2010) Proteomic profiling of nuclei from native renal inner medullary collecting duct cells using LC-MS/MS. *Physiol. Genomics* **40**, 167–183
17. Rinschen, M. M., Yu, M. J., Wang, G., Boja, E. S., Hoffert, J. D., Pisitkun, T., and Knepper, M. A. (2010) Quantitative phosphoproteomic analysis reveals vasopressin V2-receptor-dependent signaling pathways in renal collecting duct cells. *Proc. Natl. Acad. Sci. USA* **107**, 3882–3887
18. Wiśniewski, J. R., and Mann, M. (2012) Consecutive proteolytic digestion in an enzyme reactor increases depth of proteomic and phosphoproteomic analysis. *Anal. Chem.* **84**, 2631–2637
19. Thingholm, T. E., and Larsen, M. R. (2009) The use of titanium dioxide micro-columns to selectively isolate phosphopeptides from proteolytic digests. *Methods Mol. Biol.* **527**, 57–66, xi
20. Washburn, M. P., Wolters, D., and Yates III, J. R. (2001) Large-scale analysis of the yeast proteome by multidimensional protein identification technology. *Nat. Biotechnol.* **19**, 242–247

21. Cox, J., and Mann, M. (2008) MaxQuant enables high peptide identification rates, individualized p.p.b.-range mass accuracies and proteome-wide protein quantification. *Nat. Biotechnol.* **26**, 1367–1372
22. Xiao, K., Sun, J., Kim, J., Rajagopal, S., Zhai, B., Villén, J., Haas, W., Kovacs, J. J., Shukla, A. K., Hara, M. R., Hernandez, M., Lachmann, A., Zhao, S., Lin, Y., Cheng, Y., Mizuno, K., Ma'ayan, A., Gygi, S. P., and Lefkowitz, R. J. (2010) Global phosphorylation analysis of beta-arrestin-mediated signaling downstream of a seven transmembrane receptor (7TMR). *Proc. Natl. Acad. Sci. USA* **107**, 15299–15304
23. Dennis, G., Jr., Sherman, B. T., Hosack, D. A., Yang, J., Gao, W., Lane, H. C., and Lempicki, R. A. (2003) DAVID: database for annotation, visualization, and integrated discovery. *Genome Biol.* **4**, P3
24. Douglass, J., Gunaratne, R., Bradford, D., Saeed, F., Hoffert, J. D., Steinbach, P. J., Knepper, M. A., and Pisitkun, T. (2012) Identifying protein kinase target preferences using mass spectrometry. *Am. J. Physiol. Cell Physiol.* **303**, C715–C727
25. Hornbeck, P. V., Zhang, B., Murray, B., Kornhauser, J. M., Latham, V., and Skrzypek, E. (2015) PhosphoSitePlus, 2014: mutations, PTMs and recalibrations. *Nucleic Acids Res.* **43**, D512–D520
26. Schenk, L. K., Schulze, U., Henke, S., Weide, T., and Pavenstadt, H. (2016) TMEM16F regulates baseline phosphatidyserine exposure and cell viability in human embryonic kidney cells. *Cell Physiol. Biochem.* **38**, 2452–2463
27. Janji, B., Giganti, A., De Corte, V., Catillon, M., Bruyneel, E., Lentz, D., Plastino, J., Gettemans, J., and Friederich, E. (2006) Phosphorylation on Ser5 increases the F-actin-binding activity of α -plactin and promotes its targeting to sites of actin assembly in cells. *J. Cell Sci.* **119**, 1947–1960
28. Campbell, R. E., Tour, O., Palmer, A. E., Steinbach, P. A., Baird, G. S., Zacharias, D. A., and Tsien, R. Y. (2002) A monomeric red fluorescent protein. *PNAS* **99**, 7877–7882
29. Nilufar, S., Morrow, A. A., Lee, J. M., and Perkins, T. J. (2013) FiloDetect: automatic detection of filopodia from fluorescence microscopy images. *BMC Syst. Biol.* **7**, 66
30. Saleem, M. A., O'Hare, M. J., Reiser, J., Coward, R. J., Inward, C. D., Faren, T., Xing, C. Y., Ni, L., Mathieson, P. W., and Mundel, P. (2002) A conditionally immortalized human podocyte cell line demonstrating nephrin and podocin expression. *J. Am. Soc. Nephrol.* **13**, 630–638
31. Shin, S. Y., Kim, T., Lee, H. S., Kang, J. H., Lee, J. Y., Cho, K. H., and Kim, D. H. (2014) The switching role of β -adrenergic receptor signalling in cell survival or death decision of cardiomyocytes. *Nat. Commun.* **5**, 5777
32. Humphrey, S. J., Azimifar, S. B., and Mann, M. (2015) High-throughput phosphoproteomics reveals *in vivo* insulin signaling dynamics. *Nat. Biotechnol.* **33**, 990–995
33. Ayoub, M. A., Trebaux, J., Vallaghe, J., Charrier-Savournin, F., Al-Hosaini, K., Gonzalez Moya, A., Pin, J. P., Pflieger, K. D., and Trinquet, E. (2014) Homogeneous time-resolved fluorescence-based assay to monitor extracellular signal-regulated kinase signaling in a high-throughput format. *Front. Endocrinol. (Lausanne)* **5**, 94
34. Rinschen, M. M., Schroeter, C. B., Koehler, S., Ising, C., Schermer, B., Kann, M., Benzing, T., and Brinkkoetter, P. T. (2016) Quantitative deep mapping of the cultured podocyte proteome uncovers shifts in proteostatic mechanisms during differentiation. *Am. J. Physiol. Cell Physiol.* **311**, C404–C417
35. Christensen, G. L., Kelstrup, C. D., Lyngsø, C., Sarwar, U., Bøgebo, R., Sheikh, S. P., Gammeltoft, S., Olsen, J. V., and Hansen, J. L. (2010) Quantitative phosphoproteomics dissection of seven-transmembrane receptor signaling using full and biased agonists. *Mol. Cell. Proteomics* **9**, 1540–1553
36. Yao, J., Le, T. C., Kos, C. H., Henderson, J. M., Allen, P. G., Denker, B. M., and Pollak, M. R. (2004) Alpha-actinin-4-mediated FSGS: an inherited kidney disease caused by an aggregated and rapidly degraded cytoskeletal protein. *PLoS Biol.* **2**, e167
37. Morgan, A. J., and Jacob, R. (1994) Ionomycin enhances Ca^{2+} influx by stimulating store-regulated cation entry and not by a direct action at the plasma membrane. *Biochem. J.* **300**, 665–672
38. Reiser, J., von Gersdorff, G., Loos, M., Oh, J., Asanuma, K., Giardino, L., Rastaldi, M. P., Calvaresi, N., Watanabe, H., Schwarz, K., Faul, C., Kretzler, M., Davidson, A., Sugimoto, H., Kalluri, R., Sharpe, A. H., Kreidberg, J. A., and Mundel, P. (2004) Induction of B7-1 in podocytes is associated with nephrotic syndrome. *J. Clin. Invest.* **113**, 1390–1397
39. Lommel, M. J., Trairatphan, P., Gäbler, K., Laurini, C., Müller, A., Kaoma, T., Vallar, L., Sauter, T., and Schaffner-Reckinger, E. (2016) α -Plactin Ser5 phosphorylation in breast cancer cells and *in vitro* is mediated by RSK downstream of the ERK/MAPK pathway. *FASEB J.* **30**, 1218–1233
40. Al Tanoury, Z., Schaffner-Reckinger, E., Halavatyi, A., Hoffmann, C., Moes, M., Hadzic, E., Catillon, M., Yatskou, M., and Friederich, E. (2010) Quantitative kinetic study of the actin-bundling protein α -plactin and of its impact on actin turn-over. *PLoS One* **5**, e9210
41. Sapkota, G. P., Cummings, L., Newell, F. S., Armstrong, C., Bain, J., Frodin, M., Grauert, M., Hoffmann, M., Schnapp, G., Steegmaier, M., Cohen, P., and Alessi, D. R. (2007) BI-D1870 is a specific inhibitor of the p90 RSK (ribosomal S6 kinase) isoforms *in vitro* and *in vivo*. *Biochem. J.* **401**, 29–38
42. Davies, S. P., Reddy, H., Caivano, M., and Cohen, P. (2000) Specificity and mechanism of action of some commonly used protein kinase inhibitors. *Biochem. J.* **351**, 95–105
43. Poppe, H., Rybalkin, S. D., Rehmann, H., Hinds, T. R., Tang, X. B., Christensen, A. E., Schwede, F., Genieser, H. G., Bos, J. L., Doskeland, S. O., Beavo, J. A., and Butt, E. (2008) Cyclic nucleotide analogs as probes of signaling pathways. *Nat. Methods* **5**, 277–278
44. Touleec, D., Pianetti, P., Coste, H., Bellevergue, P., Grand-Perret, T., Ajakane, M., Baudet, V., Boissin, P., Boursier, E., Loriolle, F., Duhamel, L., Charon, D., and Kirilovsky, J. (1991) The bisindolylmaleimide GF 109203X is a potent and selective inhibitor of protein kinase C. *J. Biol. Chem.* **266**, 15771–15781
45. Delanote, V., Vanloo, B., Catillon, M., Friederich, E., Vandekerckhove, J., and Gettemans, J. (2010) An alpaca single-domain antibody blocks filopodia formation by obstructing α -plactin-mediated F-actin bundling. *FASEB J.* **24**, 105–118
46. Namba, Y., Ito, M., Zu, Y., Shigesada, K., and Maruyama, K. (1992) Human T cell α -plactin bundles actin filaments in a calcium-dependent manner. *J. Biochem.* **112**, 503–507
47. Ishida, H., Jensen, K. V., Woodman, A. G., Hyndman, M. E., and Vogel, H. J. (2017) The calcium-dependent switch helix of α -plactin regulates actin bundling. *Sci. Rep.* **7**, 40662
48. Brähler, S., Yu, H., Suleiman, H., Krishnan, G. M., Saunders, B. T., Kopp, J. B., Miner, J. H., Zinselmeyer, B. H., and Shaw, A. S. (2016) Intravital and kidney slice imaging of podocyte membrane dynamics. *J. Am. Soc. Nephrol.* **27**, 3285–3290
49. Greka, A., and Mundel, P. (2012) Calcium regulates podocyte actin dynamics. *Semin. Nephrol.* **32**, 319–326
50. Gloy, J., Henger, A., Fischer, K. G., Nitschke, R., Mundel, P., Bleich, M., Schollmeyer, P., Greger, R., and Pavenstädt, H. (1997) Angiotensin II depolarizes podocytes in the intact glomerulus of the rat. *J. Clin. Invest.* **99**, 2772–2781
51. Harding, S. D., Armit, C., Armstrong, J., Brennan, J., Cheng, Y., Haggarty, B., Houghton, D., Lloyd-MacGilp, S., Pi, X., Roochun, Y., Sharghi, M., Tindal, C., McMahon, A. P., Gottesman, B., Little, M. H., Georgas, K., Aronow, B. J., Potter, S. S., Brunskill, E. W., Southard-Smith, E. M., Mendelsohn, C., Baldock, R. A., Davies, J. A., and Davidson, D. (2011) The GUDMAP database—an online resource for genitourinary research. *Development* **138**, 2845–2853
52. McMahon, A. P., Aronow, B. J., Davidson, D. R., Davies, J. A., Gaido, K. W., Grimmond, S., Lessard, J. L., Little, M. H., Potter, S. S., Wilder, E. L., and Zhang, P.; GUDMAP project. (2008) GUDMAP: the genitourinary developmental molecular anatomy project. *J. Am. Soc. Nephrol.* **19**, 667–671
53. Famulski, K. S., Reeve, J., de Freitas, D. G., Kreepala, C., Chang, J., and Halloran, P. F. (2013) Kidney transplants with progressing chronic diseases express high levels of acute kidney injury transcripts. *Am. J. Transplant.* **13**, 634–644
54. Courcelles, M., Frémin, C., Voisin, L., Lemieux, S., Meloche, S., and Thibault, P. (2013) Phosphoproteome dynamics reveal novel ERK1/2 MAP kinase substrates with broad spectrum of functions. *Mol. Syst. Biol.* **9**, 669
55. Ron, D., and Kazanietz, M. G. (1999) New insights into the regulation of protein kinase C and novel phorbol ester receptors. *FASEB J.* **13**, 1658–1676
56. Khurana, S., and George, S. P. (2011) The role of actin bundling proteins in the assembly of filopodia in epithelial cells. *Cell Adhes. Migr.* **5**, 409–420
57. Rinschen, M. M., Grahammer, F., Hoppe, A. K., Kohli, P., Hagmann, H., Kretz, O., Bertsch, S., Höhne, M., Göbel, H., Bartram, M. P., Gandhirajan, R. K., Krüger, M., Brinkkoetter, P. T., Huber, T. B., Kann, M., Wickström, S. A., Benzing, T., and Schermer, B. (2017) YAP-mediated mechanotransduction determines the podocyte's response to damage. *Sci. Signal.* **10**, eaaf8165
58. Huling, J. C., Pisitkun, T., Song, J. H., Yu, M. J., Hoffert, J. D., and Knepper, M. A. (2012) Gene expression databases for kidney epithelial cells. *Am. J. Physiol. Renal Physiol.* **302**, F401–F407
59. Azatov, M., Goicoechea, S. M., Otey, C. A., and Upadhyaya, A. (2016) The actin crosslinking protein palladin modulates force generation and mechanosensitivity of tumor associated fibroblasts. *Sci. Rep.* **6**, 28805

Received for publication February 17, 2017.

Accepted for publication July 17, 2017.

Angiotensin II regulates phosphorylation of actin-associated proteins in human podocytes

Laura K. Schenk, Annika Möller-Kerutt, Rafael Klosowski, et al.

FASEB J published online August 2, 2017

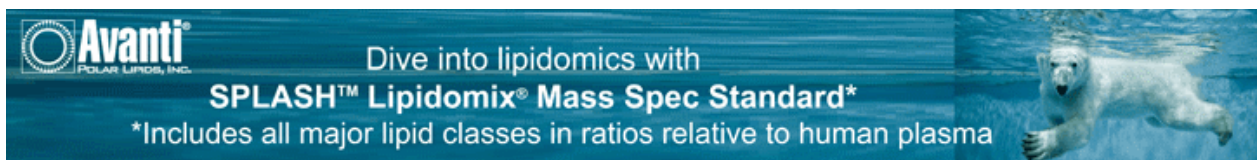
Access the most recent version at doi:[10.1096/fj.201700142R](https://doi.org/10.1096/fj.201700142R)

Supplemental Material <http://www.fasebj.org/content/suppl/2017/08/02/fj.201700142R.DC1>

Subscriptions Information about subscribing to *The FASEB Journal* is online at <http://www.faseb.org/The-FASEB-Journal/Librarian-s-Resources.aspx>

Permissions Submit copyright permission requests at: <http://www.fasebj.org/site/misc/copyright.xhtml>

Email Alerts Receive free email alerts when new an article cites this article - sign up at <http://www.fasebj.org/cgi/alerts>



Avanti
POLAR LIPIDS, INC.

Dive into lipidomics with
SPLASH™ Lipidomix® Mass Spec Standard*

*Includes all major lipid classes in ratios relative to human plasma